Article:
Zhu, Y., Yun, X. and Gardner, L. (2023) Cross-sectional behaviour and design of normal and high strength steel welded I-sections under compression and uniaxial bending. Advances in Structural Engineering, 26 (12). pp. 2228-2247. ISSN: 1369-4332

https://doi.org/10.1177/13694332231158177

Special Issue: Research into High Strength and Ultra-High Strength Steel in Advances in Structural Engineering

Advances in Structural Engineering

Advances in Structural Engineering
2023, Vol. 0(0) 1–20

DOI: 10.1177/13694332231158177
journals.sagepub.com/home/ase
SAGE

Cross-sectional behaviour and design of normal and high strength steel welded I-sections under compression and uniaxial bending

Yufei Zhu[1], Xiang Yun[2] and Leroy Gardner[1]

Abstract

A comprehensive numerical investigation into the cross-sectional behaviour and ultimate capacity of non-slender welded I-sections, made of both normal and high strength steels (NSS and HSS), under combined compression and uniaxial bending is presented. Finite element (FE) models were initially established and validated against test results collected from the literature. Subsequently, parametric studies were conducted using the validated FE models to generate extensive numerical data considering different steel grades, cross-section geometries and loading combinations. The obtained numerical data, together with the test results collected from the literature, were utilised to assess the accuracy of the traditional European (EC3) and North American (AISC) design provisions, as well as the Continuous Strength Method (CSM), for NSS and HSS welded I-sections under combined loading. The assessment indicated that the CSM was able to provide more accurate and consistent resistance predictions than the current EC3 and AISC design provisions owing to its ability to capture the spread of plasticity and strain hardening in a systematic, mechanics-based manner. Finally, the reliability levels of the different design methods were statistically evaluated in accordance with EN 1990:2002.

Keywords

Combined loading, Continuous Strength Method, Cross-section design, Finite element modelling, High strength steels, Normal strength steels, Parametric studies, Welded I-sections

Introduction

High strength steels (HSS), with nominal yield strengths equal to or greater than 460 MPa, are being increasingly used in the construction industry. Compared with traditional normal strength steels (NSS), the inherent high strength-to-weight ratio of HSS brings a range of benefits, such as reduced dimensions of structural members, lower transportation and handling costs, less required welding and painting and, overall, reduced consumption of non-renewable resources (Baddoo and Chan, 2017). The current European design provisions for HSS structural elements are set out in EN 1993-1-12 (2007), which mirror the design rules specified in EN 1993-1-1 (2005, 2019) for NSS structures. EN 1993-1-12 (2007) is currently applicable to the design of structural members made of steel grades up to S700, while there are presently no design rules that can be directly applied to structural members made of ultra-HSS (e.g. S960). To date, a series of investigations (Cao et al., 2020; Shi et al., 2014, 2015; Su et al., 2021a; Sun et al., 2019) have been carried out to study the cross-sectional behaviour and design of HSS welded I-section stub columns made of steel grades up to 960 MPa. Regarding welded I-sections under combined loading, Sun et al. (2021) investigated the cross-sectional behaviour of S690 non-slender (i.e. Class 1 to Class 3 according to EN 1993-1-12 (2007)) welded I-section stub columns subjected to compression plus major or minor axis bending by means of experimental and numerical analyses. Su et al. (2021, 2021b)

[1]Department of Civil and Environmental Engineering, Imperial College London, London, UK
[2]Department of Civil and Structural Engineering, The University of Sheffield, Sheffield, UK

Corresponding author:
Xiang Yun, Department of Civil and Structural Engineering, The University of Sheffield, Sir Frederick Mappin Building (Broad Lane Building), Sheffield S1 3JD, UK.
Email: x.yun@sheffield.ac.uk

carried out both experimental and numerical programmes to examine the local stability of slender (i.e. Class 4 according to EN 1993-1-12 (2007)) S960 welded I-section stub columns subjected to compression plus major or minor axis bending. These studies have concluded that EN 1993-1-12 (2007) generally yields conservative resistance predictions for HSS welded I-sections under combined loading.

The ultimate resistances of welded steel I-sections under combined loading are generally influenced by both plasticity and local instability, with the latter being increasingly dominant with increasing cross-sectional slenderness (Shi et al., 2016). Yun et al. (2023) studied the member buckling behaviour of welded I-section columns, made of a wide range of steel grades, and devised a modified Eurocode 3 (EC3) design approach that accounted for the varying influence of steel strength and residual stresses. To the authors' knowledge, no equivalent systematic study to explore the influence of steel grade on the cross-sectional behaviour of welded I-sections under combined loading has yet been conducted; this is therefore the focus of the present study. This paper aims to characterise the local buckling behaviour and ultimate resistance of non-slender welded I-sections, made of steel grades varying from 355 MPa to 960 MPa, under combined compression and uniaxial bending. FE models were firstly established and validated against existing test results collected from the literature (Su et al., 2021, 2021b; Sun et al., 2021), and then employed to carry out parametric studies to generate supplementary numerical data covering a wide range of steel grades, cross-section geometries and loading combinations. Based on the numerically derived data, together with the test results collected from the literature (Sun et al., 2021), the current cross-section design provisions specified in EN 1993-1-1 (2005, 2019), EN 1993-1-12 (2007) and AISC 360-16 (2016), as well as the Continuous Strength Method (CSM) (Gardner and Nethercot, 2004; Gardner, 2008; Gardner et al., 2023; Yun et al., 2018b), were evaluated for both NSS and HSS non-slender welded I-sections under combined compression and uniaxial bending. Finally, reliability analysis was performed to evaluate the reliability levels of the different design methods according to EN 1990:2002 (2002).

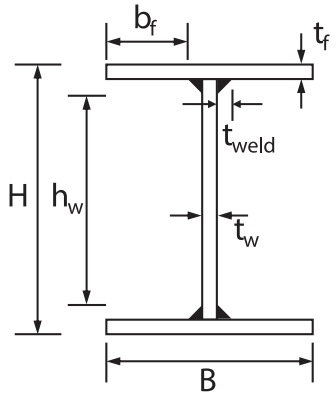

Figure 1. Notation of geometry of modelled welded I-sections.

Numerical modelling

The cross-sectional behaviour of NSS and HSS welded I-sections under combined compression and uniaxial bending was numerically investigated using the FE analysis package ABAQUS (2018). The notation of the geometries of the modelled welded I-sections is shown in Figure 1, where B is the overall flange width, H is the outer section depth, t_f is the flange thickness, t_w is the web thickness, t_{weld} is the weld leg length, b_f is the clear width of the outstand flange (i.e. $b_f = (B\text{-}t_w)/2\text{-}t_{weld}$), and h_w is the clear height of the web (i.e. $h_w = H\text{-}2t_f\text{-}2t_{weld}$). The basic modelling assumptions are described in the first subsection. The developed FE models were validated against existing test results collected from the literature (Su et al., 2021, 2021b; Sun et al., 2021), as presented the second subsection, and utilised in parametric studies to generate extensive numerical results for a broad range of steel grades, cross-section geometries and loading combinations, as described the third subsection.

Basic modelling assumptions

The four-noded doubly curved shell element S4R with reduced integration and finite membrane strains has been extensively and successfully used in previous numerical investigations of NSS and HSS welded I-section structural elements (Yun et al., 2022; Zhu et al., 2023), and was also employed in the present study for the modelling of welded I-section stub columns. An element size approximately equal to $(B + H)/40$ was applied to the modelled stub columns in both the transverse and longitudinal directions; the adopted mesh size was shown to be able to capture the cross-section buckling response with reasonable computational efficiency. For validation purposes, the weld fillets of the I-sections were carefully modelled by means of five finer mesh elements with equal height but different widths, as shown in Figure 2. Nodes at both ends of the web were offset from the web-to-flange junctions by half the flange thickness $t_f/2$ in order to avoid any overlap between the flange and web plates, as illustrated in Figure 2. The same mesh density as that employed in the present work has been successfully used for the modelling of welded I-section structural elements in previous studies (Yun et al., 2022; Zhu et al., 2023).

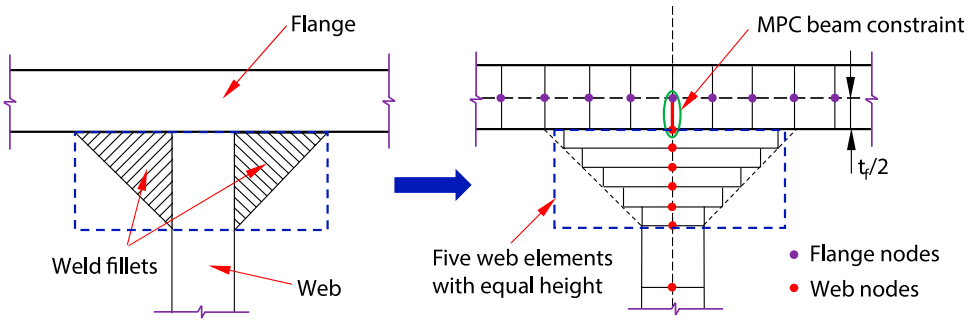

Figure 2. Modelling approach for representing weld fillets in welded I-sections.

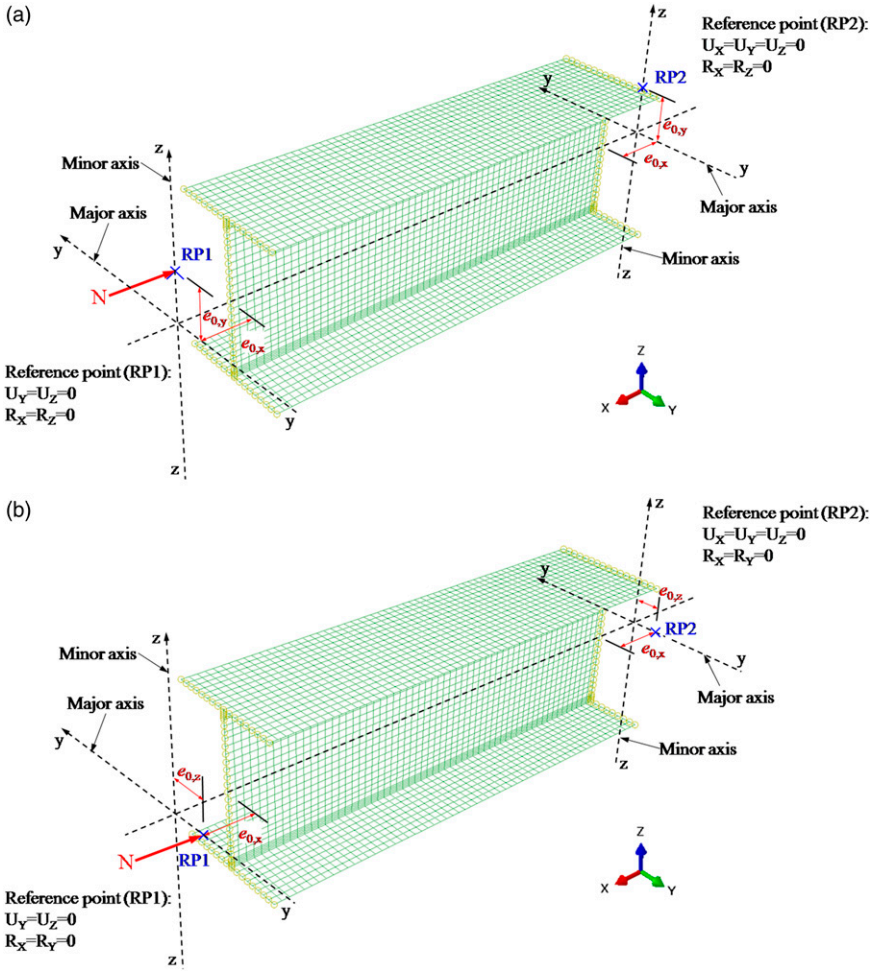

Figure 3. Boundary conditions employed in finite element models of welded I-section stub columns subjected to compression plus uniaxial bending.

The modelled specimens were loaded through knife edges. A reference point representing the tip of the knife edge (i.e. the loading/reaction point) was created at each end section of the stub column FE models, as shown in Figure 3; the reference point was offset from the centroid of the end section laterally by a distance equal to the applied loading eccentricity (i.e. $e_{0,y}$ and $e_{0,z}$ for major axis bending and minor axis bending, respectively, as indicated in Figure 3)

and longitudinally by the total thickness of the knife edge, wedge plate and end plate according to the test setup in (Su et al., 2021, 2021b; Sun et al., 2021) for model validation (i.e. $e_{0,x}$ as shown in Figure 3). The nodes at each end section of the stub column FE model were coupled to the corresponding reference point by means of kinematic coupling, with pinned in-plane and fixed out-of-plane boundary conditions assigned to the reference point. With regards to material properties for validation, the measured engineering stress-strain relationships obtained from tensile coupon tests reported in (Su et al., 2021, 2021b; Sun et al., 2021) were converted into true stress-logarithmic plastic strain curves before inputting into ABAQUS.

Initial local geometric imperfections were incorporated into the FE models in the form of sinusoidal half-waves of half-wavelength equal to $L/3$, where L is the length of the modelled stub column, in the longitudinal direction by means of adjusting the nodal coordinates of the original perfect geometry, as illustrated in Figure 4. The amplitudes of the local imperfections were taken as the measured values in the validation study and tolerance-based values set out in Annex C of EN1993-1-5 (2006) in the parametric studies. Specifically, the local imperfection amplitude of the flange $\omega_{0,f}$ was taken equal to 1/50 of the clear width of the outstand flange b_f when the flange plates are more susceptible to local buckling than the web plate (i.e. the elastic local buckling stress of the flange plates under uniform compression $\sigma_{cr,f}$ determined in accordance with EN 1993-1-5 (2006) is lower than that of the web plate $\sigma_{cr,w}$); otherwise, the local imperfection amplitude of the web $\omega_{0,w}$ was adopted as 1/200 of the clear height of the web h_w when the web plate is more susceptible to local buckling than the flange plates (i.e. $\sigma_{cr,f} > \sigma_{cr,w}$). The local imperfection amplitude for the constituent plate that is less susceptible to local buckling can then be determined according to the compatibility requirement that the angle at the web-to-flange junctions of the modelled I-sections remained at 90°, as indicated in Figure 4.

Residual stresses were incorporated into the FE models using the residual stress pattern put forward by Yun et al. (2023) for both NSS and HSS welded I-sections. The residual stress pattern (Yun et al., 2022a) was developed based on the statistical analysis of a large number of existing residual stress measurements collected from the literature, as shown in Figure 5, where $\sigma_{r,ft}$ and $\sigma_{r,wt}$ are the maximum tensile residual stresses in the flanges and the web, respectively, and $\sigma_{r,fc}$ and $\sigma_{r,wc}$ are the maximum compressive residual stresses in the flanges and the web, respectively. Note that compressive and tensile residual stresses are denoted as negative and positive values, respectively, as indicated in Figure 5. The maximum tensile residual stresses (i.e. $\sigma_{r,ft}$ or $\sigma_{r,wt}$) can be predicted using equation (1) or equation (2), which correspond to the mean or upper characteristic (i.e. 95th percentile) values from the analysed residual stress data. As recommended in (Yun et al., 2022a), the residual stress pattern with the mean value of the maximum tensile residual stresses predicted by equation (1) can be used for validating FE models, while the residual stress pattern with the upper characteristic value of the maximum tensile residual stresses predicted by equation (2) should be used in parametric studies in order to generate safe-sided structural performance data. The residual stress model has been successfully employed in previous numerical studies of NSS and HSS welded I-section beams (Zhu et al., 2023) and columns (Yun et al., 2022a). A separate analysis step was created in order to achieve self-equilibrium of the residual stresses prior to the application of the external loading. The modified Riks method (Hibbitt et al., 1997), which is able to obtain nonlinear static equilibrium solutions for unstable problems, was adopted in order to capture the full load-deformation (including post-peak) response of the stub columns subjected to compression plus uniaxial bending.

$$\frac{\sigma_{r,wt}(\sigma_{r,ft})}{f_y} = -0.5 \times \sqrt{\frac{f_y}{235}} + 1.32 \leq 1 \quad (1)$$

$$\frac{\sigma_{r,wt}(\sigma_{r,ft})}{f_y} = -0.5 \times \sqrt{\frac{f_y}{235}} + 1.5 \leq 1 \quad (2)$$

Validation of FE models

The accuracy of the developed FE models was verified through comparisons of the numerical results, in terms of the ultimate loads, load-lateral deformation histories and failure modes, with those obtained from physical tests (Su et al., 2021, 2021b; Sun et al., 2021). For test specimens whose weld leg lengths were not reported, the nominal values as recommended in Section J2 of AISC 360-16 (2016) were utilised in the FE models for validation purposes. Both measured and tolerance-based local imperfection amplitudes were incorporated into the FE models with the aims of assessing the sensitivity of the developed FE models to variation in local imperfection amplitudes and examining the suitability of the tolerance-based local imperfection amplitudes for use in the parametric studies.

Tables 1 and 2 summarise the comparisons of the numerically derived ultimate loads $N_{u,FE}$ with those obtained from the experiments $N_{u,test}$ for stub columns under compression plus major axis bending and minor axis bending, respectively. The mean values of the FE-to-test ultimate loads and the corresponding coefficients of variation (COV) are also reported in Tables 1 and 2. The

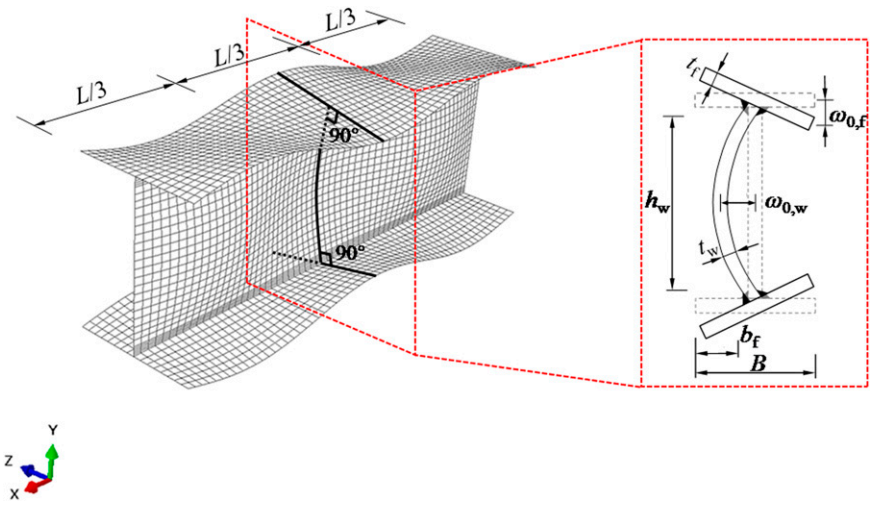

Figure 4. Form and amplitudes of local geometric imperfections employed in finite element models.

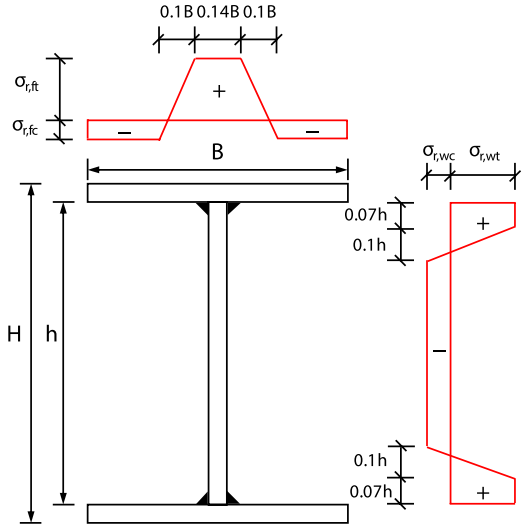

Figure 5. Residual stress pattern adopted in finite element models.

comparisons indicate that the developed FE models can provide generally accurate resistance predictions when the measured local imperfection amplitudes are utilised, while the use of the tolerance-based local imperfection amplitudes in the FE models results in slightly conservative resistance predictions. The load-mid-height lateral deformation histories obtained from the tests were closely simulated by the established FE models, as shown in Figure 6 for four representative specimens. The failure modes observed in the tests were also successfully replicated by their FE counterparts, typical examples of which are displayed in Figure 7. It can therefore be confirmed that the developed FE models can accurately simulate the local buckling behaviour of welded I-section stub columns subjected to compression plus uniaxial bending and are thus suitable for use in subsequent parametric studies.

Parametric studies

Upon validation of the developed FE models, parametric studies were performed to generate extensive numerical data covering a broad range of steel grades, cross-section geometries and loading combinations. Four steel grades, from normal strength to high strength – S355, S460, S690 and S960, were considered in the parametric studies. The bilinear plus nonlinear hardening material model proposed by Yun and Gardner (2017) for hot-rolled steels was used for the description of the full-range stress-strain curves for the S355, S460 and S690 steels, while the average measured stress-strain curve obtained from the longitudinal tensile coupon tests (ABAQUS, 2021) was adopted for the S960 steel since only a limited number of experimental stress-strain curves on S960 steel were available at the time when the bilinear plus nonlinear hardening material model was developed. The key material properties of the four investigated steel grades, including the Young's modulus E, the yield strength f_y and the ultimate tensile strength f_u, are summarised in Table 3, and the adopted full-range engineering stress-strain curves are plotted in Figure 8.

Regarding the cross-section dimensions of the modelled welded I-sections, the flange width B was fixed at 100 mm, while the outer section depths H were taken as 100 mm, 150 mm and 200 mm, resulting in three different cross-section aspect ratios H/B of 1.0, 1.5 and 2.0. For each cross-section aspect ratio, three different values of flange thickness t_f, varying from 5.6 mm to

Table 1. Comparison of experimental and numerical ultimate loads for welded I-section stub columns under compression plus major axis bending.

		$N_{u,FE}/N_{u,test}$	
		Local imperfection amplitudes	
Steel grade	Specimen label	Measured values	Tolerance-based values
S690 (Sun et al., 2021)	MA-1	1.00	0.99
	MA-2	1.02	1.02
	MA-3	0.98	0.98
	MA-4	0.98	0.96
	MA-5	1.03	0.98
S960 (Su et al., 2021b)	A1	1.01	0.92
	A2	1.00	0.89
	A3	0.98	0.89
	A4	1.04	0.94
	A5	1.02	0.93
	B1	1.00	0.93
	B2	0.99	0.93
	B3	1.00	0.90
	B4	1.00	0.91
	B5	0.99	0.93
	Mean	1.00	0.94
	COV	0.018	0.042

Table 2. Comparison of experimental and numerical ultimate loads for welded I-section stub columns under compression plus minor axis bending.

		$N_{u,FE}/N_{u,test}$	
		Local imperfection amplitudes	
Steel grade	Specimen label	Measured values	Tolerance-based values
S690 (Sun et al., 2021)	MI-1	0.99	0.98
	MI-2	0.98	0.98
	MI-3	0.99	0.99
	MI-4	0.94	0.94
	MI-5	0.96	0.95
S960 (Su et al., 2021)	A1	0.99	0.91
	A2	0.99	0.91
	A3	1.00	0.91
	A4	0.95	0.88
	A5	0.99	0.92
	B1	0.98	0.98
	B2	0.98	0.98
	B3	0.98	0.97
	B4	0.99	0.99
	B5	0.98	0.98
	Mean	0.98	0.95
	COV	0.016	0.038

14 mm, and web thickness t_w, varying from 3.4 mm to 20 mm, were selected to achieve a spectrum of local slenderness covering all three non-slender cross-section classes (i.e. Class 1–3) on the basis of the slenderness limits set out in EN 1993-1-1 (2005, 2019) and EN 1993-1-12 (2007). For each modelled welded I-section, the flange and web thicknesses were specified such that the web plate slenderness $\overline{\lambda}_{p,w}$ in compression determined in accordance with EN 1993-1-5 (2006) was approximately equal to that of the flange plate $\overline{\lambda}_{p,f}$, thus limiting the

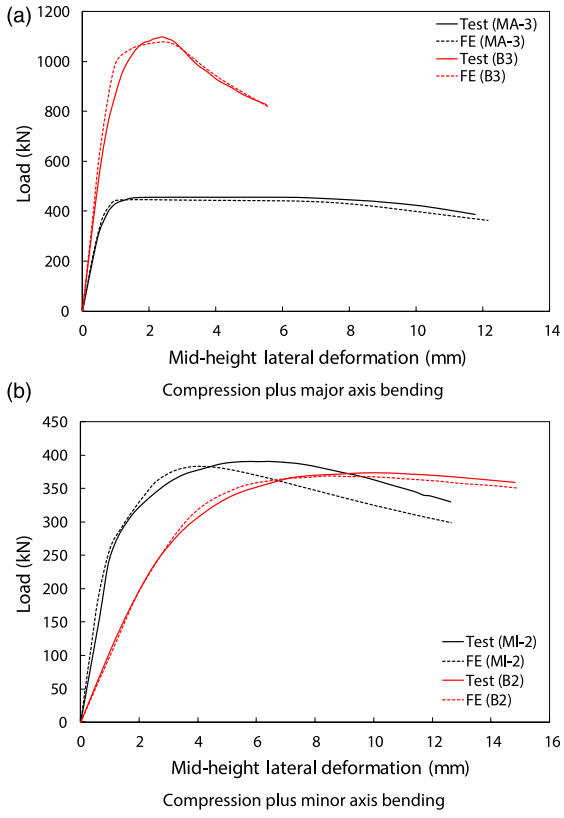

Figure 6. Comparison of experimental (Su et al., 2021, 2021b; Sun et al., 2021) and numerical load-mid-height deformation histories for stub column specimens subjected to compression plus uniaxial bending.

effects of plate element interaction on the local buckling behaviour of the welded I-sections. The weld fillets were ignored for all the modelled welded I-section stub columns in the parametric studies for simplicity and modelling convenience. The length of each stub column model was set equal to three times the average outer cross-section dimension (i.e. $(B + H)/2$) (Ziemian, 2010). The tolerance-based local imperfection amplitudes, combined with the upper characteristic amplitudes of the residual stresses (using equation (2)), were employed throughout the parametric studies.

The initial loading eccentricities for each modelled welded I-section in both the major and minor axis directions were varied between 0.8 mm and 691 mm so that a broad variety of loading combinations could be obtained. In total, 1320 numerical results on NSS and HSS welded I-sections under compression plus uniaxial bending were generated through the parametric studies, comprising 648 data for compression plus major axis bending and 672 for compression plus minor axis bending.

Stability design of welded I-sections under compression plus uniaxial bending

In this section, the accuracy of the European (EC3) (2005, 2007, 2019) and North American (AISC) (2016) design provisions, as well as a newly proposed CSM-based design approach (Yun et al., 2018b), for NSS and HSS non-slender welded I-sections subjected to combined compression and uniaxial bending is assessed using the FE data derived from the parametric studies and the test results collected from (Sun et al., 2021). The assessment was performed by comparing the FE (or test) ultimate loads $N_{u,FE(test)}$ against the ultimate loads predicted using the different design methods $N_{u,pred}$, as reported in Tables 4 and 5 for welded I-sections subjected to combined compression plus major and minor axis bending, respectively. Note that the subscripts FE and FE(test) used throughout the present article indicate that only FE data or both FE and test data have been used in the analysis, respectively. A ratio of $N_{u,FE(test)}/N_{u,pred}$ greater than unity indicates that the design method provides a safe-sided resistance prediction. Note that all partial safety factors (γ_{M0} and ϕ) have been set equal to 1.0 and omitted from the design equations presented in this section to facilitate a direct comparison between the FE (or test) ultimate loads and the design predictions; reliability analyses are carried out in the next section. In the following subsections, the three different design methods are briefly presented and their accuracy for the stability design of NSS and HSS welded I-sections under combined loading is discussed.

European codes EN 1993-1-1 and EN 1993-1-12 (EC3)

The current EC3 design provisions for HSS structures are given in EN 1993-1-12 (2007). The rules largely follow those set out in EN 1993-1-1 (2005, 2019) for NSS structures; no distinction is made between NSS and HSS in the local stability and cross-section checks. In addition, EN 1993-1-12 (2007) is applicable to steel grades up to S700, thus no design rules are offered for steel members made of ultra-HSS (e.g. S960). In this subsection, the accuracy and applicability of the current EC3 design provisions for both NSS and HSS (up to S960) welded I-sections subjected to combined compression and bending are assessed.

EN 1993-1-1 (2005) adopts a linear interaction formula for the design of Class 3 (i.e. semi-compact) welded I-sections under compression plus major axis

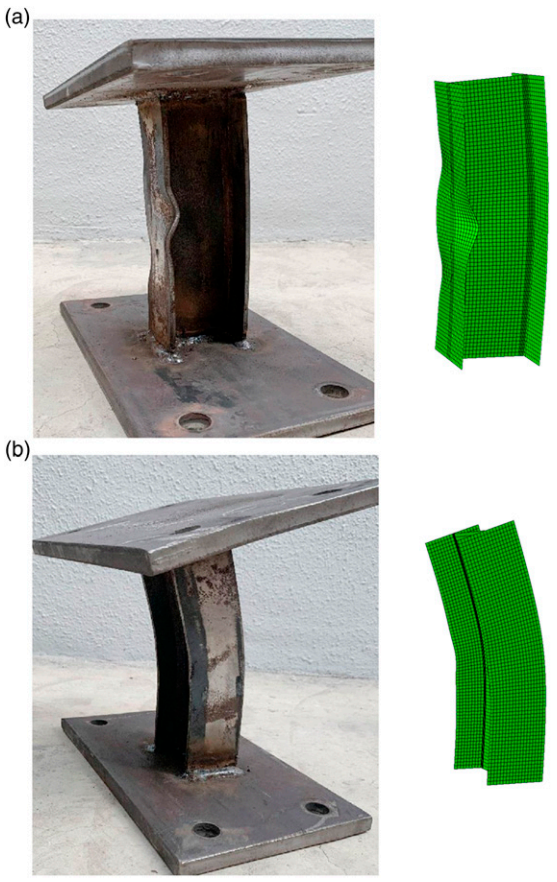

Figure 7. Comparison of experimental and numerical failure modes for stub columns subjected to compression plus uniaxial bending.

bending and a nonlinear interaction formula for compression plus minor axis bending. In the latest draft of the new version of this code, prEN 1993-1-1 (2019), the same interaction formulae are used, but with the concept of an elasto-plastic moment introduced — see equations (3) and (4).

$$\frac{N_{\mathrm{Ed}}}{N_{\mathrm{y,\,EC3}}}+\frac{M_{\mathrm{Ed}}}{M_{\mathrm{ep,\,y}}}\leq 1 \tag{3}$$

$$\left(\frac{N_{\mathrm{Ed}}}{N_{\mathrm{y,\,EC3}}}\right)^{2}+\frac{M_{\mathrm{Ed}}}{M_{\mathrm{ep,\,z}}}\leq 1 \tag{4}$$

In equations (3) and (4), N_{Ed} is the design axial load, M_{Ed} is the design bending moment about the considered axis of bending, with due account taken of second order effects, $N_{\mathrm{y,EC3}}$ is the cross-sectional yield load in pure compression, equal to the product of the gross cross-sectional area A and the yield strength f_{y}, and $M_{\mathrm{ep,y}}$ and $M_{\mathrm{ep,z}}$ are the cross-sectional elasto-plastic bending resistances about the major and minor axes, respectively, equal to the product of the elasto-plastic section modulus W_{ep} about the considered axis of bending and the yield strength f_{y}. It should be noted that, according to prEN 1993-1-1 (2019), the cross-sectional bending resistance for Class 3 welded I-sections can be taken conservatively as the traditional elastic moment resistance M_{el} (i.e. the product of the elastic section modulus W_{el} and the yield strength f_{y}), or alternatively as the elasto-plastic moment resistance M_{ep}; the latter is employed in the assessments presented herein since it provides more accurate cross-sectional bending resistance predictions for Class 3 welded I-sections due to the consideration of the partial spread of plasticity.

The elasto-plastic section modulus W_{ep} is determined from an interpolation between the plastic section modulus W_{pl} and the elastic section modulus W_{el} about

Table 3. Key material properties for S355, S460, S690 and S960 steels employed in parametric studies.

Steel grade	E	f_y	f_u
	N/mm^2	N/mm^2	N/mm^2
S355	210000	355	490
S460	210000	460	540
S690	210000	690	770
S960	204393	969	1024

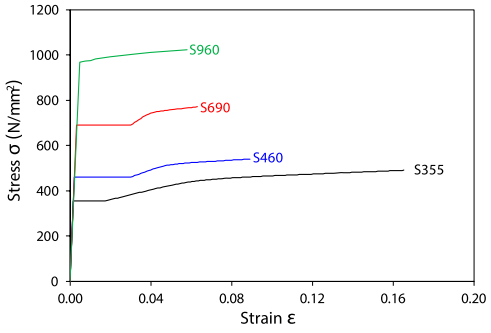

Figure 8. Full-range stress-strain curves for S355, S460, S690 and S960 steels employed in parametric studies.

the considered axis of bending, as given by equation (5)

$$W_{ep} = W_{pl} - (W_{pl} - W_{el})\beta_{ep} \tag{5}$$

where β_{ep} is a coefficient related to the material parameter $\varepsilon = \sqrt{235/f_y}$ and the width-to-thickness ratios b_f/t_f and h_w/t_w, as given by equations (6) and (7) for the major and minor axis bending, respectively.

$$\beta_{ep,y} = \text{Max}\left(\frac{b_f/t_f - 10\varepsilon}{4\varepsilon}, \frac{h_w/t_w - 83\varepsilon}{38\varepsilon}, 0\right), \text{but } \beta_{ep,y} \le 1.0 \tag{6}$$

$$\beta_{ep,z} = \text{Max}\left(\frac{b_f/t_f - 10\varepsilon}{6\varepsilon}, 0\right), \text{but } \beta_{ep,z} \le 1.0 \tag{7}$$

A bilinear interaction formula, as given by equation (8), is employed for the design of Class 1 and 2 welded I-sections under compression plus major axis bending, while a nonlinear interaction formula, as given by equation

Table 4. Comparison of finite element and test results with different resistance predictions for normal strength steels and high strength steel welded I-sections under compression plus major axis bending.

Steel grade	No. of FE data (Test data)	Evaluation parameter	$N_{u,FE(test)}/N_{u,pred,EC3}$	$N_{u,FE(test)}/N_{u,pred,AISC}$	$N_{u,FE(test)}/N_{u,pred,csm}$
S355	162	Mean	1.113	1.124	1.125
		COV	0.160	0.179	0.146
		Max.	1.443	1.507	1.444
		Min.	0.916	0.919	0.951
S460	162	Mean	1.072	1.084	1.097
		COV	0.103	0.118	0.099
		Max.	1.293	1.356	1.337
		Min.	0.922	0.929	0.959
S690	162 (5)	Mean	1.034	1.046	1.062
		COV	0.050	0.057	0.045
		Max.	1.166	1.181	1.212
		Min.	0.931	0.947	0.985
S960	162	Mean	1.041	1.052	1.080
		COV	0.046	0.039	0.038
		Max.	1.193	1.157	1.180
		Min.	0.946	0.974	1.001
Overall	648 (5)	Mean	1.065	1.077	1.091
		COV	0.107	0.119	0.097
		Max.	1.443	1.507	1.444
		Min.	0.916	0.919	0.951

Table 5. Comparison of finite element and test results with different resistance predictions for normal strength steels and High strength steels welded I-sections under compression plus minor axis bending.

Steel grade	No. of FE data (Test data)	Evaluation parameter	$N_{u,FE(test)}/N_{u,pred,EC3}$	$N_{u,FE(test)}/N_{u,pred,AISC}$	$N_{u,FE(test)}/N_{u,pred,csm}$
S355	168	Mean	1.059	1.279	1.092
		COV	0.146	0.130	0.117
		Max.	1.516	1.655	1.520
		Min.	0.868	1.009	0.963
S460	168	Mean	1.029	1.251	1.070
		COV	0.094	0.091	0.067
		Max.	1.268	1.464	1.283
		Min.	0.860	1.026	0.972
S690	168 (5)	Mean	1.018	1.248	1.064
		COV	0.078	0.078	0.051
		Max.	1.166	1.475	1.233
		Min.	0.860	1.054	0.972
S960	168	Mean	1.022	1.263	1.086
		COV	0.073	0.077	0.038
		Max.	1.175	1.509	1.200
		Min.	0.837	1.093	1.011
Overall	672 (5)	Mean	1.032	1.260	1.078
		COV	0.104	0.097	0.075
		Max.	1.516	1.655	1.520
		Min.	0.837	1.009	0.963

(9), is utilised for those subjected to compression plus minor axis bending.

$$M_{R,EC3,y} = M_{pl,y}\frac{1-n}{1-0.5a} \leq M_{pl,y} \tag{8}$$

$$M_{R,EC3,z} = M_{pl,z}\left[1-\left(\frac{n-a}{1-a}\right)^2\right] \leq M_{pl,z} \tag{9}$$

In equations (8) and (9), $M_{R,EC3,y}$ and $M_{R,EC3,z}$ are the EC3 design bending resistances about the major and minor axis, respectively, considering the influence of the presence of the axial compression N_{Ed}, $M_{pl,y}$ (i.e. the product of the plastic section modulus about the major axis $W_{pl,y}$ and the yield strength f_y) and $M_{pl,z}$ (i.e. the product of the plastic section modulus about the minor axis $W_{pl,y}$ and the yield strength f_y) are the cross-sectional plastic bending resistances about the major and minor axes, respectively, n is the axial load ratio equal to $N_{Ed}/(Af_y)$ and a is the ratio of the web-to-gross cross-section area (i.e. $(A- 2t_f B)/A$) with an upper limit of 0.5.

The accuracy of the EC3 interaction formulae (Equations (8) and (9)) for NSS and HSS welded I-sections under combined compression plus uniaxial bending was assessed based on the FE and test data. A graphical assessment was carried out, as shown in Figures 9 and 10 for welded I-sections subjected to compression plus major axis and minor axis bending, respectively, where the FE and test ultimate bending moments $M_{u,FE(test)}$ (calculated considering second order effects) and axial loads $N_{u,FE(test)}$ are normalised by their respective plastic bending resistances M_{pl} and yield loads N_{pl}, and are compared with the EC3 interaction curves. Note that the EC3 interaction curves depend on geometry-related parameters, such as the ratio of the web-to-gross cross-section area a for Class 1 and 2 welded I-sections and the ratio of the elasto-plastic-to-plastic section modulus W_{ep}/W_{pl} for Class 3 welded I-sections; thus, the average interaction curves determined based on the average geometric properties of the investigated welded I-sections are plotted in Figures 9 and 10 for illustration purposes. As shown in Figures 9 and 10, for Class 1 and 2 welded I-sections, the EC3 interaction curves generally yield conservative resistance predictions particularly for stockier welded I-sections made of lower steel grades (i.e. S355 and S460 steels which exhibit a higher degree of strain hardening than the S690 and S960 steels). The overall conservatism under combined loading is attributed principally to the conservatism in the predictions of the cross-sectional compression and bending resistances (serving as the end points of the interaction curves) arising from the beneficial influence of strain hardening being neglected. However, there are also a large number of data points lying on the unsafe side for Class 1 and 2 welded I-sections with less stocky cross-sections, especially for those subjected to compression plus minor axis bending, as shown in Figure 10; this stems largely from the shape of the interaction curves, which feature a fixed plateau length

of $0.5a$ for welded I-sections subjected to compression plus major axis bending and a for welded I-sections subjected to compression plus minor axis bending. For Class 3 welded I-sections, both the linear (for compression plus major axis bending) and the nonlinear (for compression plus minor axis bending) interaction curves yield accurate resistance predictions, as shown in Figures 9 and 10, resulting from the use of accurate bending end points (i.e. elasto-plastic bending resistance M_{ep}) and suitable forms of interaction curves. It can also be seen from Figures 9 and 10 that for less stocky welded I-sections (i.e. Class 2 welded I-sections whose slendernesses approach the Class 3 limits and Class 3 welded I-sections), the influence of the steel grade on the cross-sectional buckling resistances is seen to be negligible since there is no or little strain hardening experienced.

In addition, the ratios of the FE and test ultimate loads $N_{u,FE(test)}$ to the ultimate capacities predicted by EC3 $N_{u,pred,EC3}$ are plotted against the cross-section slenderness $\overline{\lambda}_p$ in Figure 11(a) and (b) for specimens subjected to compression plus major axis bending and minor axis bending, respectively. The cross-section slenderness $\overline{\lambda}_p$ quantifies the susceptibility of a cross-section to local buckling and is defined as the square root of the yield stress f_y divided by the local elastic buckling stress of the full cross-section $\sigma_{cr,cs}$, as given in equation (10).

$$\overline{\lambda}_p = \sqrt{\frac{f_y}{\sigma_{cr,cs}}} \tag{10}$$

The full cross-section local buckling stress $\sigma_{cr,cs}$ can be determined either using the empirical formulae of Gardner et al. (2019), as adopted in the present study, or using numerical tools such as CUFSM (Schafer and Adany, 2006). It can be observed from Figures 9–11 that the EC3 design approach provides somewhat inaccurate and scattered resistance predictions for welded I-sections subjected to compression plus uniaxial bending, which is evidenced by the statistical results summarised in Tables 4 and 5. For very stocky welded I-sections, whose cross-sectional responses are dominated by yielding, stub columns made of NSS are able to achieve higher normalised ultimate capacities than their HSS counterparts, primarily due to the higher level of strain hardening of NSS. However, the differences in the normalised ultimate capacities between stub columns made of NSS and HSS become small for less stocky welded I-sections with $\overline{\lambda}_p > 0.35$ since failure occurs before strain hardening is experienced. Therefore, there is significant scope for improvements to the current EC3 design approach; this can be done by improving the accuracy of the cross-sectional compression and bending resistances, which act as the end points of the design interaction curve, and by modifying the shape of the interaction curve based on the more accurate end points, as discussed the following subsection.

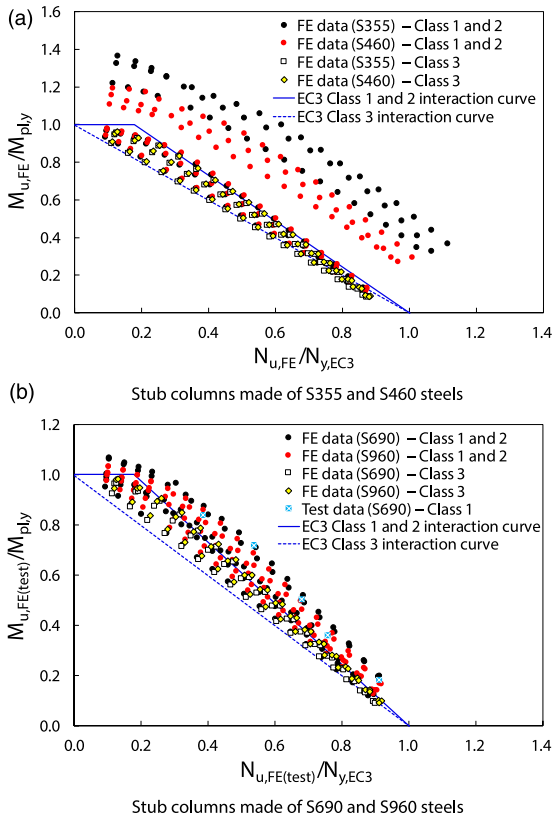

Figure 9. Comparison of normalised finite element and test results with average EC3 interaction curves for normal strength steels and high strength steels welded I-sections under compression plus major axis bending.

American specification AISC 360-16 (AISC)

The American specification AISC 360-16 (2016) employs a bilinear interaction curve, as expressed by equation (11), for the design of non-slender welded I-sections under combined loading, where N_{AISC} is the nominal cross-sectional compression resistance and M_{AISC} is the nominal cross-sectional bending resistances about the considered axis of bending. The nominal compression resistance of a non-slender welded I-section (i.e. equivalent to a Class 1–3 welded I-section according to EC3) N_{AISC} is calculated through multiplying the gross cross-sectional area A by the flexural buckling stress f_{cr}. Compared to the EC3 cross-sectional yield load $N_{y,EC3}$, the yield strength f_y is replaced by the flexural buckling stress f_{cr} to determine the AISC cross-sectional compression resistance N_{AISC}, which accounts for the influence of the second order effects, though these are minimal for short members, as studied herein. The flexural

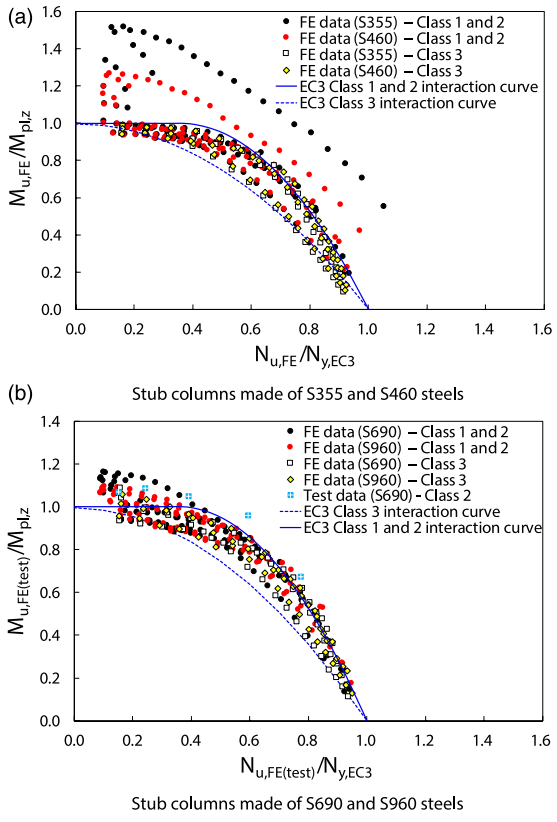

Figure 10. Comparison of normalised finite element and test results with average EC3 interaction curves for normal strength steels and high strength steels welded I-sections under compression plus minor axis bending.

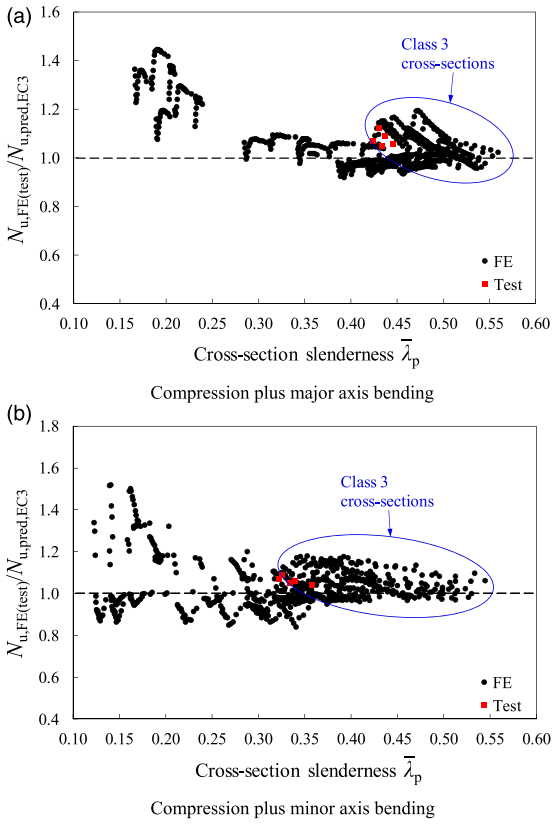

Figure 11. Comparison of finite element and test results with EC3 resistance predictions for normal strength steels and high strength steels welded I-section stub columns subjected to compression plus uniaxial bending.

buckling stress f_{cr} were calculated in accordance with Section E3 of AISC 360-16 (2016). The nominal cross-sectional bending resistances M_{AISC} were determined according to Sections F3 and F6 of AISC 360-16 (2016), which employ the plastic bending resistances M_{pl} for compact welded I-sections (i.e. equivalent to Class 1 and 2 welded I-sections in EC3) and elasto-plastic bending resistances allowing for the partial spread of plasticity for semi-compact welded I-sections (i.e. equivalent to Class 3 welded I-sections in EC3).

$$\begin{cases} \dfrac{N_{Ed}}{N_{AISC}} + \dfrac{8}{9}\dfrac{M_{Ed}}{M_{AISC}} \le 1.0 & \text{for} \dfrac{N_{Ed}}{N_{AISC}} \ge 0.2 \\ \dfrac{N_{Ed}}{2N_{AISC}} + \dfrac{M_{Ed}}{M_{AISC}} \le 1.0 & \text{for} \dfrac{N_{Ed}}{N_{AISC}} < 0.2 \end{cases} \quad (11)$$

The accuracy of the AISC interaction formula (equation (11)) for NSS and HSS welded I-sections subjected to compression plus uniaxial bending was assessed based on the FE and test results. The FE and test ultimate bending moments $M_{u,FE(test)}$ (considering second order effects) and axial loads $N_{u,FE(test)}$ are normalised by their respective AISC cross-sectional bending resistances M_{AISC} and compression resistances N_{AISC}, and are compared with the AISC interaction curve (equation (11)), as shown in Figures 12 and 13 for welded I-sections subjected to compression plus major axis and minor axis bending, respectively. It should be noted that, due to the different cross-section classification frameworks employed in EC3 and AISC, all the welded I-sections investigated in the present study are classified as compact cross-sections according to AISC. For the EC3 Class 1 and 2 welded I-sections, the AISC bilinear interaction curves provide more conservative resistance predictions than EC3, whose interaction curves feature a plateau in the region with lower axial load ratios. For the EC3 Class 3 welded I-sections, AISC yields less conservative strength predictions for the case of compression plus major axis bending, though there are a number of data points appearing on the unsafe side, as shown in Figure 12, but provides rather conservative resistance predictions for the case of compression plus minor axis bending, as shown in Figure 13, compared to EC3.

The ratios of the FE and test ultimate loads $N_{u,FE(test)}$ to the ultimate resistances predicted by AISC $N_{u,pred,AISC}$ are plotted against the cross-section slenderness $\overline{\lambda}_p$ in Figure 14(a) and (b) for welded I-sections subjected to

compression plus major axis bending and minor axis bending, respectively. As shown in Figure 14, the AISC design method generally yields conservative and rather scattered resistance predictions; the overall mean ratios of $N_{u,FE(test)}/N_{u,pred,AISC}$ are equal to 1.077 and 1.260, with the COV of 0.119 and 0.097, for all the investigated NSS and HSS welded I-sections subjected to compression plus major axis bending and minor axis bending, respectively, as reported in Tables 4 and 5. The key sources of the deviations between FE/test and predicted results are (1) the conservative predictions of the cross-sectional compression and bending resistances (serving as the end points of the AISC interaction curve) due to strain hardening being neglected, especially for very stocky welded I-sections and (2) the adoption of a single interaction curve for non-slender welded I-sections with different cross-section slenderness $\overline{\lambda}_p$ subjected to different loading configurations.

New CSM-based design proposals

On the basis of the previous evaluations, it is generally revealed that the existing design methods provide somewhat inaccurate and scattered resistance predictions for NSS and HSS welded I-sections subjected to compression plus uniaxial bending. Yun et al. (2018b) proposed an improved design approach, based on the CSM (Yun et al., 2018a) for the calculation of cross-sectional compression and bending resistances and the general format of the EC3 interaction formula, for NSS hot-rolled steel I-sections under combined loading (Yun et al., 2018b). In this subsection, a new design method, based on (Yun et al., 2018b), is proposed for NSS and HSS welded I-sections subjected to compression plus uniaxial bending.

The design method proposed for NSS hot-rolled steel I-sections under combined loading (Yun et al., 2018b) utilises the CSM compression and bending resistances as the end points, which have been shown to be more accurate than the EC3 and AISC predictions (Yun et al., 2018a). The CSM is a deformation-based method that enables a rational allowance of material nonlinearity (i.e. the spread of plasticity and strain hardening) in determining the cross-sectional resistances of steel structural elements. The CSM consists of two fundamental components – a 'base curve' that defines the limiting strain ε_{csm} that a cross-section can resist prior to failure and a constitutive model that allows for the influence of strain hardening. The limiting strain ε_{csm} for a given non-slender welded I-section (i.e. $\overline{\lambda}_p \leq 0.68$ (Afshan and Gardner, 2013)) can be determined from equation (12), where ε_y is the material yield strain equal to f_y/E, ε_u is the strain corresponding to the material ultimate tensile stress f_u and $\overline{\lambda}_p$ is the cross-section slenderness

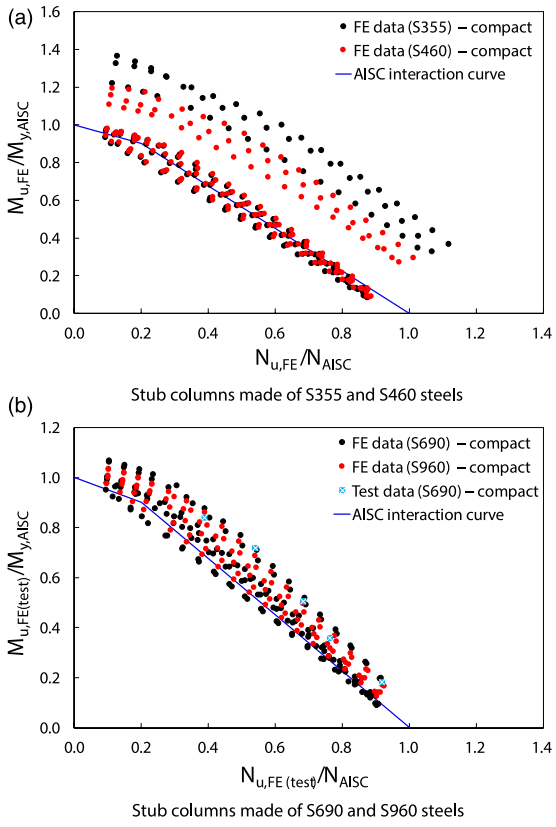

Figure 12. Comparison of normalised finite element and test results with the North American interaction curves for normal strength steels and high strength steels welded I-sections under compression plus major axis bending.

defined by equation (10). Two upper bounds are applied to the strain ratio $\varepsilon_{csm}/\varepsilon_y$: the first limit of Ω is set to prevent excessive strains and defines the permissible level of plastic deformation on project-by-project basis, with a recommended value of 15, in line with the EN 1993-1-1 ductility requirement (Gardner et al., 2023); the second limit of $C_1\varepsilon_u/\varepsilon_y$, where C_1 is a coefficient corresponding to the adopted quad-linear material model as described in the following paragraphs (Yun and Gardner, 2017; Yun et al., 2018a), defines a cut-off strain (restricting strains to the first three stages of the quad-linear material model described below) to avoid over-predictions of material strength when using the adopted resistance functions.

$$\frac{\varepsilon_{csm}}{\varepsilon_y} = \frac{0.25}{\overline{\lambda}_p^{3.6}} \leq \min\left(\Omega, \frac{C_1\varepsilon_u}{\varepsilon_y}\right) \text{ for } \overline{\lambda}_p \leq 0.68 \qquad (12)$$

A quad-linear material model, proposed by Yun and Gardner (2017), has been employed throughout the recent development of the CSM for the design of NSS and HSS structural elements. The quad-linear material model is

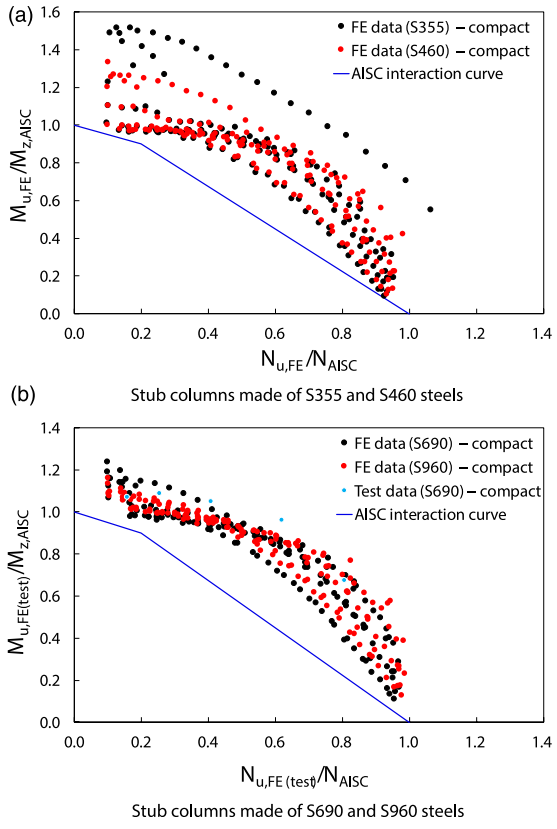

Figure 13. Comparison of normalised finite element and test results with the North American interaction curves for normal strength steels and high strength steels welded I-sections under compression plus minor axis bending.

shown in Figure 15 and defined by equation (13), where ε and σ are the engineering strain and stress, respectively, ε_{sh} is the strain hardening strain at which the material yield plateau ends and strain hardening initiates and E_{sh} is the strain hardening modulus defined as the slope of the third linear stage of the model that passes through the strain hardening point (ε_{sh}, f_y) and a specified maximum point ($C_2\varepsilon_u$, f_u), as shown in Figure 15.

$$\sigma = \begin{cases} E\varepsilon & \text{for } \varepsilon \le \varepsilon_y \\ f_y & \text{for } \varepsilon_y < \varepsilon \le \varepsilon_{sh} \\ f_y + E_{sh}(\varepsilon - \varepsilon_{sh}) & \text{for } \varepsilon_{sh} < \varepsilon \le C_1\varepsilon_u \\ f_{C_1\varepsilon_u} + \dfrac{f_u - f_{C_1\varepsilon_u}}{\varepsilon_u - C_1\varepsilon_u}(\varepsilon - C_1\varepsilon_u) & \text{for } C_1\varepsilon_u < \varepsilon \le \varepsilon_u \end{cases} \quad (13)$$

Two coefficients are adopted in the quad-linear material model: the first coefficient C_1 defines the transition strain (i.e. $C_1\varepsilon_u$) to the fourth stage of the quad-linear model, and the second coefficient C_2 is used to define the strain hardening modulus E_{sh}, as given by

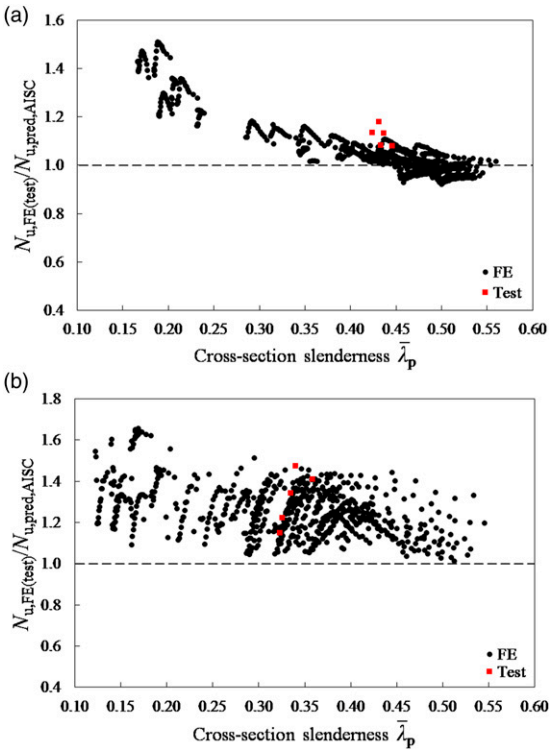

Figure 14. Comparison of finite element and test results with North American resistance predictions for normal strength steels and high strength steels welded I-section stub columns subjected to compression plus uniaxial bending.

$$E_{sh} = \frac{f_u - f_y}{C_2\varepsilon_u - \varepsilon_{sh}} \quad (14)$$

The parameters ε_u, ε_{sh}, C_1 and C_2 used in the quad-linear material model can be determined from the predictive expressions of equations (15)–(18), respectively.

$$\varepsilon_u = 0.6\left(1 - \frac{f_y}{f_u}\right), \text{but } \varepsilon_u \ge 0.06 \quad (15)$$

$$\varepsilon_{sh} = 0.1\frac{f_y}{f_u} - 0.055, \text{but } 0.015 \le \varepsilon_{sh} \le 0.03 \quad (16)$$

$$C_1 = \frac{\varepsilon_{sh} + 0.25(\varepsilon_u - \varepsilon_{sh})}{\varepsilon_u} \quad (17)$$

$$C_2 = \frac{\varepsilon_{sh} + 0.4(\varepsilon_u - \varepsilon_{sh})}{\varepsilon_u} \quad (18)$$

Within the CSM design framework, hot-rolled NSS and HSS cross-sectional resistances are determined utilising the limiting strain ε_{csm} obtained from the CSM base curve (equation (12)), in conjunction with the quad-

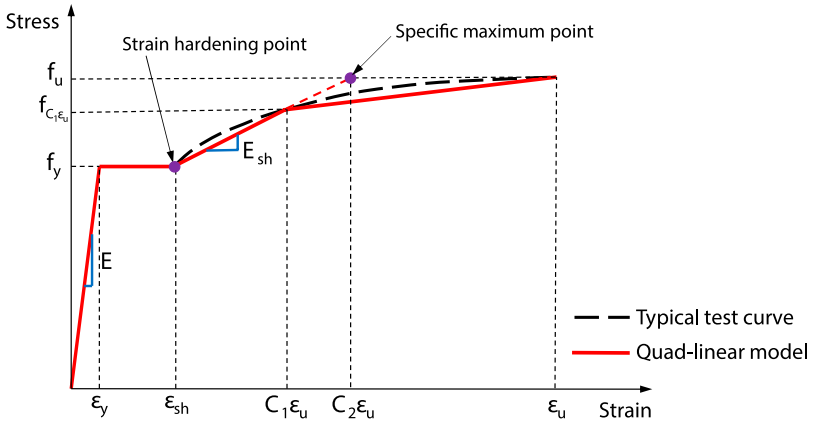

Figure 15. Typical test stress-strain curve and the quad-linear model for normal strength steels and high strength steels (Yun and Gardner, 2017).

linear material model. The CSM cross-sectional compression resistance N_{csm} is calculated as the product of the gross cross-sectional area A and the CSM limiting stress σ_{csm}, as given by equation (19). The CSM limiting stress σ_{csm} is determined by substituting $\varepsilon = \varepsilon_{csm}$ into the expression of the quad-linear material model as given in equation (13).

$$N_{csm} = A\sigma_{csm} \tag{19}$$

For non-slender (i.e. Class 1–3) NSS and HSS welded I-sections, the CSM bending resistance M_{csm} is determined by equation (20) when strain hardening is not experienced (i.e. $\varepsilon_{csm} < \varepsilon_{sh}$) and equation (21) for stockier cross-sections whose CSM limiting strain ε_{csm} exceeds the strain hardening strain ε_{sh} and strain hardening is experienced. In equations (20) and (21), α and β are dimensionless coefficients that are equal to 1.2 and 0.05 for I-sections bending about their minor axis, respectively, and equal to 2 and 0.08 for I-sections bending about their major axis, respectively.

$$M_{csm} = W_{pl} f_y \left[1 - \left(1 - \frac{W_{el}}{W_{pl}}\right) \Big/ \left(\frac{\varepsilon_{csm}}{\varepsilon_y}\right)^{\alpha}\right]$$

$$\text{for NSS and HSS non} - \text{slender welded I} - \text{sections whose } \varepsilon_{csm} \le \varepsilon_{sh} \tag{20}$$

$$M_{csm} = W_{pl} f_y \left[1 - \left(1 - \frac{W_{el}}{W_{pl}}\right) \Big/ \left(\frac{\varepsilon_{csm}}{\varepsilon_y}\right)^{\alpha} + \beta \frac{E_{sh}}{E} \left(\frac{\varepsilon_{csm} - \varepsilon_{sh}}{\varepsilon_y}\right)^{2}\right]$$

$$\text{for NSS and HSS non} - \text{slender welded I} - \text{sections whose } \varepsilon_{csm} > \varepsilon_{sh} \tag{21}$$

Yun et al. (2018b) proposed an improved design approach for NSS non-slender hot-rolled I-sections subjected to combined compression and bending moment. The proposed design approach features the use of the *N-M* interaction expressions specified in EC3 but with CSM cross-sectional compression and bending resistances as the end points, as given by equations (22) and (23) for hot-rolled I-sections with $\overline{\lambda}_p \le 0.6$ under compression plus major and minor axis bending, respectively, and by equation (24) for hot-rolled I-sections with $\overline{\lambda}_p > 0.6$ under combined compression and bending moment.

$$M_{R,csm,y} = M_{csm,y} \frac{1 - n_{csm}}{1 - 0.5 a_{csm,w}} \le M_{csm,y} \tag{22}$$

$$M_{R,csm,z} = M_{csm,z} \left[1 - \left(\frac{n_{csm} - a_{csm,f}}{1 - a_{csm,f}}\right)^2\right] \le M_{csm,z} \tag{23}$$

$$\frac{N_{Ed}}{N_{csm}} + \frac{M_{Ed}}{M_{csm}} \le 1 \tag{24}$$

In equations (22)–(24), n_{csm} is the load ratio of N_{Ed}/N_{csm}, $M_{csm,y}$ and $M_{csm,z}$ are the CSM cross-sectional bending resistances about the major and minor axis, respectively, $M_{R,csm,y}$ and $M_{R,csm,z}$ are the CSM bending resistances about the major and minor axis, respectively, considering the influence of the presence of the axial compression N_{Ed}, and $a_{csm,w}$ and $a_{csm,f}$ are parameters involving the ratios of the web area A_w and flange area A_f to the gross cross-sectional area A, as given by equations (25) and (26) respectively. The parameters $a_{csm,w}$ and $a_{csm,f}$, equivalent to the parameter a used in EC3, define the plateau lengths of the interaction curves, i.e. $0.5a_{csm,w}$ and $a_{csm,f}$ for hot-rolled I-sections under compression plus major axis bending and minor axis bending, respectively.

$$a_{csm,w} = \frac{A_w}{A} \le 0.25 \tag{25}$$

$$a_{csm,f} = \left(\frac{A_f}{A} - 0.5\right) \le 0.25, \text{ but } a_{csm,f} \ge 0 \tag{26}$$

The applicability of a similar design approach (Yun et al., 2018b) to NSS and HSS non-slender (i.e. Class 1–3)

welded I-sections under combined loading is explored in this subsection. A slight modification was made to equations (22) and (23) by introducing a reduction factor φ for the plateau length of the interaction curves (Fieber et al., 2019, 2020; Yun and Gardner, 2018; Yun et al., 2020), as given by equation (27), enabling a gradual decrease in plateau length with increasing cross-sectional slenderness $\overline{\lambda}_p$, with the plateau length of the proposed interaction curves reducing to zero for welded I-sections when $\overline{\lambda}_p$ = 0.68. The final expressions of the proposed design interaction curves are given by equations (28) and (29) for NSS and HSS welded I-sections under compression plus major and minor axis bending, respectively.

$$\varphi = 1.36 - 2\overline{\lambda}_p, \text{but } 0 \le \varphi \le 1 \tag{27}$$

$$M_{R,csm,y} = M_{csm,y}\frac{1 - n_{csm}}{1 - 0.5\varphi a_{csm,w}} \le M_{csm,y} \tag{28}$$

$$M_{R,csm,z} = M_{csm,z}\left[1 - \left(\frac{n_{csm} - \varphi a_{csm,f}}{1 - \varphi a_{csm,f}}\right)^2\right] \le M_{csm,z} \tag{29}$$

The numerically and experimentally obtained ultimate bending moments $M_{u,FE(test)}$ (considering second order effects) and axial compression loads $N_{u,FE(test)}$ are normalised by their respective CSM cross-sectional bending resistances M_{csm} and compression resistances N_{csm}, and are compared with the average proposed interaction curves (Equations (28) and (29)), as shown in Figures 16 and 17 for welded I-sections subjected to compression plus major axis and minor axis bending, respectively. It can be observed from Figures 16 and 17 that the FE and test data points follow a tighter trend for both loading cases compared to the EC3 and AISC predictions, with the majority of the data set lying above the proposed interaction curves (i.e. on the safe side).

The improved accuracy and consistency of the proposed design approach can also be seen in Figure 18(a) and (b), where the ratios of FE and test ultimate loads $N_{u,FE(test)}$ to ultimate resistances predicted by the proposed method $N_{u,pred,csm}$ are plotted against the cross-section slenderness $\overline{\lambda}_p$ for welded I-sections subjected to compression plus major axis bending and minor axis bending, respectively. As tabulated in Tables 4 and 5, the overall mean ratios of $N_{u,FE(test)}/N_{u,pred,csm}$ are equal to 1.091 and 1.078, with COV values of 0.097 and 0.075, for all the investigated NSS and HSS welded I-sections subjected to compression plus major axis bending and minor axis bending, respectively; these statistical data indicate that the design proposals presented herein result in much more consistent and accurate resistance predictions for NSS and HSS welded I-sections subjected to combined compression plus bending compared to the current codified methods of EC3 and AISC.

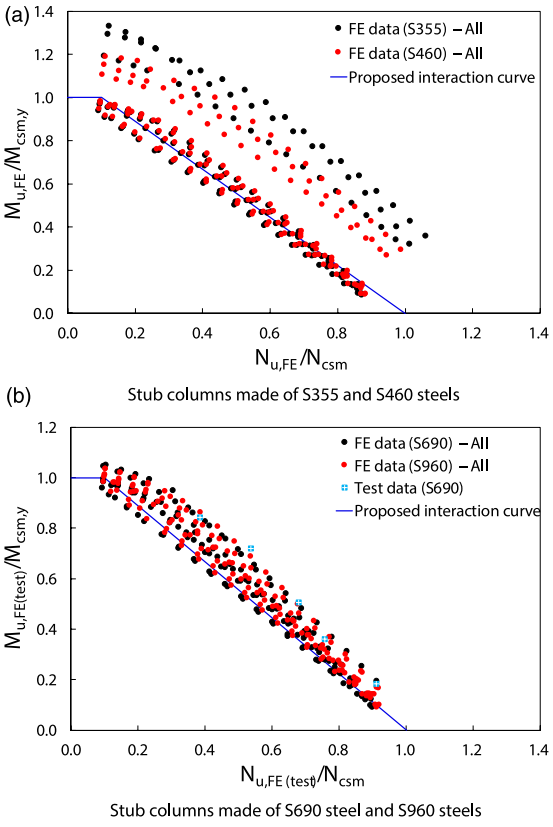

Figure 16. Comparison of normalised finite element and test results with average proposed interaction curves for normal strength steels and high strength steels welded I-sections under compression plus major axis bending.

In addition, the ratios of $N_{u,FE(test)}/N_{u,pred,csm}$ are plotted against a radial angle parameter θ in Figures 20 and 21 for welded I-sections under compression plus major and minor axis bending, respectively, in order to examine the influence of the applied loading combination (i.e. the ratio of the applied axial compression to bending moment) on the ultimate resistance predictions using the different design methods. The radial angle parameter θ is defined by equation (30) and illustrated in Figure 19, which describes the combination of axial compression load and bending moment. In equation (30), N_{Rd} and M_{Rd} are respectively the cross-sectional compression and bending resistances predicted using the different design approaches. According to this definition, θ = 0° and θ = 90° correspond to pure bending and pure compression, respectively. It can be seen from Figures 20 and 21 that the proposed design method provides the highest degree of accuracy and consistency in the resistance predictions for both NSS and HSS welded I-sections subjected to different loading combinations (i.e. $0° \le \theta \le 90°$). The proposed design method, however, still provides conservative resistance predictions, especially for very stocky welded I-sections, as indicted in Figure 18; this is due primary to the fact that the strain hardening is not

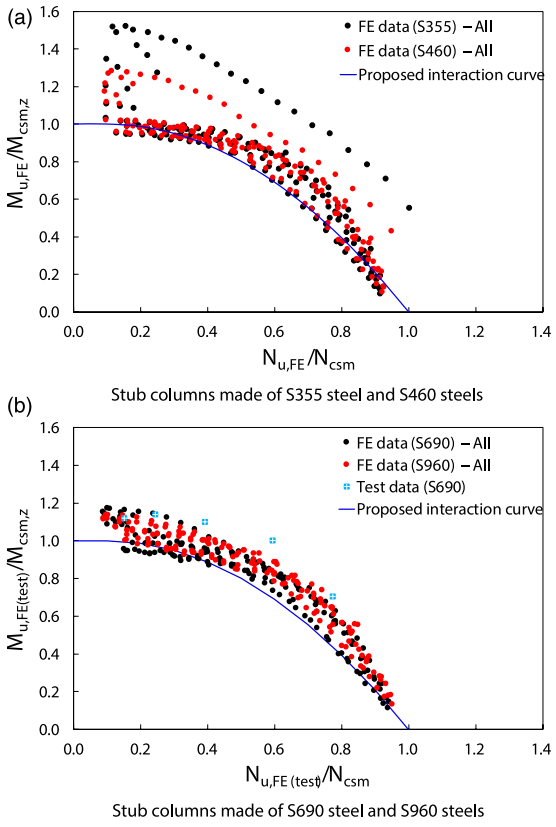

Figure 17. Comparison of normalised finite element and test results with average proposed interaction curves for normal strength steels and high strength steels welded I-sections under compression plus minor axis bending.

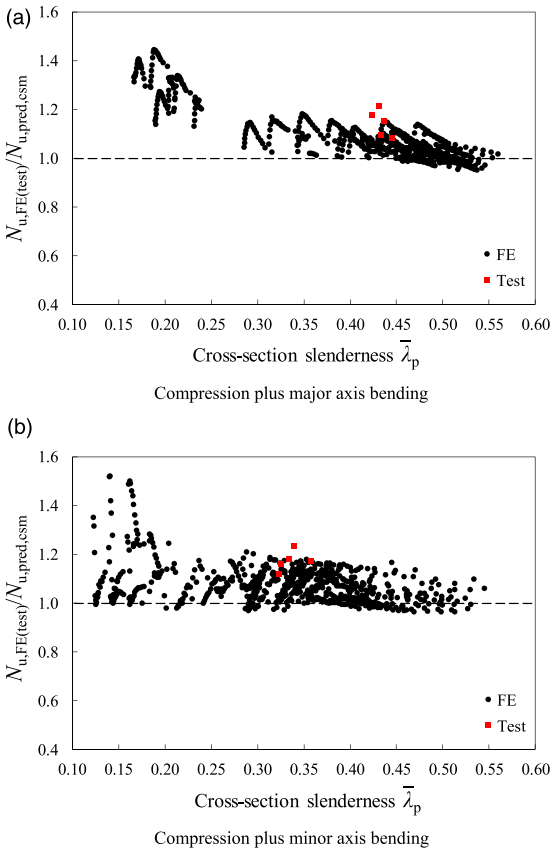

Figure 18. Comparison of finite element and test results with resistances predicted by the proposed method for normal strength steels and high strength steels welded I-section stub columns subjected to compression plus uniaxial bending.

fully exploited for very stocky welded I-sections since an upper bound to the strain limit of $\varepsilon_{csm}/\varepsilon_y = 15$ (i.e. $\Omega = 15$) is imposed. This strain limit could, however, be relaxed, especially for NSS structural elements, which exhibit good ductility, resulting in less conservative resistance predictions (Fieber et al., 2020; Yun et al., 2018b, 2020).

$$\theta = \tan^{-1}\left(\frac{N_{u,FE(test)}/N_{Rd}}{M_{u,FE(test)}/M_{Rd}}\right) \quad (30)$$

Reliability analysis

The reliability of the existing (i.e. EC3 and AISC) and proposed CSM-based design methods for NSS and HSS welded I-sections under combined compression plus uniaxial bending is assessed in this section following the procedure given in Annex D of EN 1990 (2002). The material overstrength, i.e. the mean-to-nominal yield strength ratio, were taken equal to 1.20 for S355 steel, 1.15 for S460 steel and 1.10 for S690 and S960 steels, with the corresponding COV values equal to 0.050 for S355 steel, 0.045 for S460 steel and

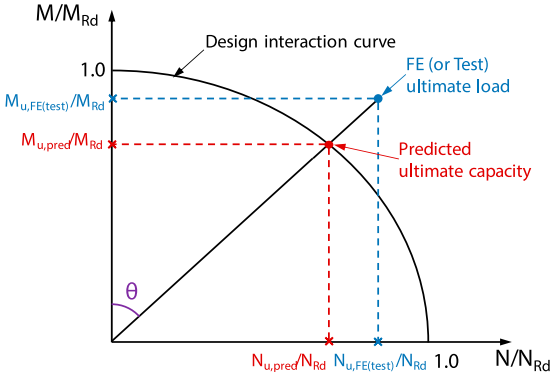

Figure 19. Graphical definition of the radial angle parameter θ used for the assessment of design methods.

0.035 for S690 and S960 steels, according to prEN 1993-1-1 (2019). The COV of the cross-sectional area V_A was calculated using the variability parameters of the basic cross-sectional dimensions (H, B, t_f and t_w) following the procedure outlined

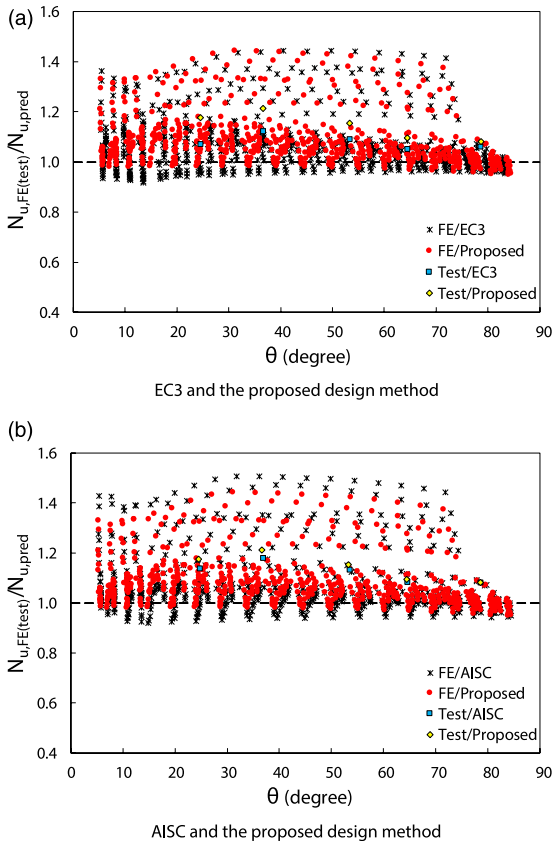

Figure 20. Assessment of accuracy of different design methods for welded I-sections under compression plus major axis bending (date arranged with respect to the radial angle parameter θ).

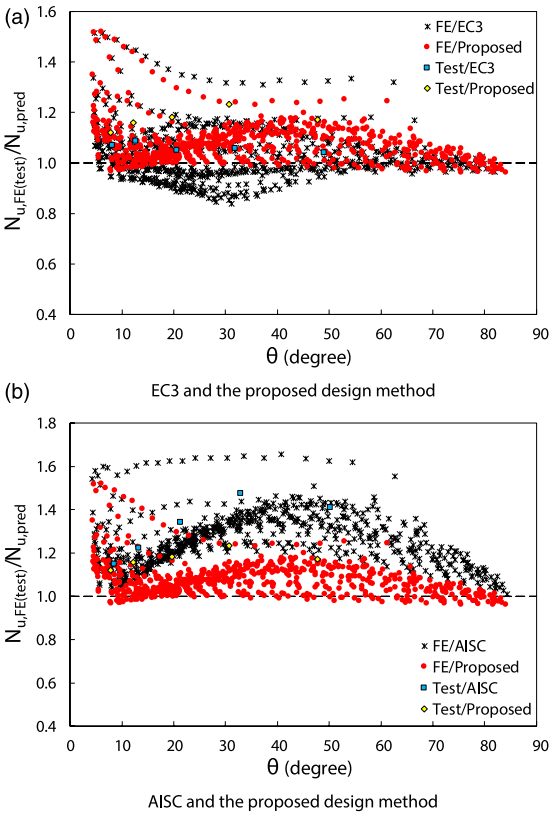

Figure 21. Assessment of accuracy of different design methods for welded I-sections under compression plus minor axis bending (date arranged with respect to the radial angle parameter θ).

in (Afshan et al., 2015), which is, on average, equal to 0.02 for the investigated welded I-sections.

The key statistical results from the reliability analyses are summarised in Table 6, where $k_{d,n}$ is the design fractile factor depending on the number of the results considered n, b is the correction factor determined from the following equation:

$$b = \frac{1}{n}\sum_{i=1}^{n}\frac{r_{e,i}}{r_{t,i}}, \tag{31}$$

in which $r_{e,i}$ is the experimental or numerical resistance and $r_{t,i}$ is the theoretical resistance predicted from the resistance model, V_δ is the COV of the test and FE resistances relative to the predictions from the resistance model, V_r is the combined COV incorporating the variability of the resistance model and the basic variables, γ^*_{M0} is the required partial safety factor, γ_{M0} is the target partial safety factor (equal to 1.0 according to prEN 1993-1-1 (2019)), and f_a is the acceptance limit on the ratio of $\gamma^*_{M0}/\gamma_{M0}$, as determined by equation (32) (da Silva et al., 2017).

$$\gamma^*_{M0}/\gamma_{M0} \le f_a = 1.03 + 0.75(V_r - 0.04), \text{but } 1.03 \le f_a \le 1.15 \tag{32}$$

Note that the correction factor b is defined as the average of the ratios of the experimental or numerical resistance $r_{e,i}$ to the theoretical resistance $r_{t,i}$ to prevent b being biased towards the experimental or numerical results with higher failure loads (Afshan et al., 2015; Meng et al., 2020), which is different from the least squares method specified in Annex D of EN 1990 (2002). A detailed description of the calculation of these key statistical can be found in (Afshan et al., 2015; Yun et al., 2022, 2022a).

It can be seen from Table 6 that the required partial safety factors γ^*_{M0} for the proposed method are equal to 1.073 and 1.094 for NSS and HSS welded I-sections subjected to compression plus major and minor axis bending, respectively; these values are close to, yet slightly higher than, the target value of 1.0 recommended in EN 1993-1-1 (2005, 2019), but are lower than the corresponding values of EC3 and AISC, except for welded I-sections subjected to compression plus minor axis bending in the case of AISC. The $(\gamma^*_{M0}/\gamma_{M0})/f_a$ ratios for

Table 6. Summary of key statistical results from reliability analyses.

Loading configuration	Design method	No. of data	$k_{d,n}$	b	V_δ	V_r	γ^*_{M0}	f_a	$(\gamma^*_{M0}/\gamma_{M0})/f_a$
Compression plus major axis bending	EC3	653	3.053	1.065	0.101	0.081	1.199	1.081	1.109
	AISC	653	3.053	1.077	0.110	0.118	1.215	1.088	1.117
	Proposed	653	3.053	1.091	0.064	0.076	1.073	1.057	1.015
Compression plus minor axis bending	EC3	677	3.053	1.032	0.099	0.106	1.218	1.080	1.128
	AISC	677	3.053	1.260	0.095	0.103	0.988	1.078	0.917
	Proposed	677	3.053	1.078	0.071	0.082	1.094	1.061	1.031

the proposed method are equal to 1.015 and 1.031 for NSS and HSS welded I-sections subjected to compression plus major and minor axis bending, respectively, which are very marginally greater than unity and may be considered to be tolerable. It can, therefore, be concluded that the proposed design method provides a higher level of reliability than the current codified design approaches (i.e. EC3 and AISC), while significantly improving the accuracy and consistency of resistance predictions for NSS and HSS welded I-sections subjected to combined compression and uniaxial bending.

Conclusions

The cross-sectional behaviour and design of NSS and HSS welded I-sections, made of steel grades varying from 355 MPa to 960 MPa, subjected to combined compression and uniaxial bending have been numerically investigated in this paper. FE models that can accurately replicate the structural response of welded I-sections under combined loading were created and validated against experimental results collected from the literature. The validated FE models were subsequently used in parametric studies to generate extensive numerical results considering a wide range of cross-section geometries, steel grades and loading combinations. A total of 1320 numerical data were derived; these numerical data, combined with the existing test results, were utilised to evaluate the accuracy of the existing European (EC3) (2005, 2007, 2019) and North American (AISC) (2016) design methods for NSS and HSS non-slender welded I-sections subjected to compression plus uniaxial bending. The assessment revealed that both the EC3 and AISC design methods yield scattered and somewhat inaccurate resistance predictions, due primarily to the omission of strain hardening in predicting the cross-sectional compression and bending resistances (i.e. the endpoints of the interaction curves) and the shapes of the interaction curves themselves. New design proposals, based on the CSM for the calculation of the end point resistances, together with newly developed interaction curves, were proposed. The new design proposals were shown to yield more accurate and consistent resistance predictions for both NSS and HSS welded I-sections under combined loading than the existing codified methods of EC3 and AISC. Finally, reliability analysis was performed on the different design methods according to Annex D of EN 1990 (2002), indicating that the new design proposals generally provide a higher level of reliability than the current codified design approaches.

Declaration of conflicting interests

The author(s) declared no potential conflicts of interest with respect to the research, authorship, and/or publication of this article.

Funding

The author(s) disclosed receipt of the following financial support for the research, authorship, and/or publication of this article: This project has received funding from the Research Fund for Coal and Steel under grant agreement no. 743504.

ORCID iDs

Yufei Zhu https://orcid.org/0000-0003-4818-8359
Xiang Yun https://orcid.org/0000-0002-5179-4731

References

ABAQUS (2018) *Version 6.14-2*. Johnston, RI: SIMULIA.

ABAQUS (2021) *ABAQUS V.6.21, Commercial FE Software and Documentation Dassault Systèmes*. Providence, RI, USA: Simulia Corporation.

Afshan S and Gardner L (2013) The continuous strength method for structural stainless steel design. *Thin-Walled Structures* 68: 42–49.

Afshan S, Francis P, Baddoo NR, et al. (2015) Reliability analysis of structural stainless steel design provisions. *Journal of Constructional Steel Research* 114: 293–304.

ANSI/AISC 360-16 (2016) *Specification for Structural Steel Buildings*.

Baddoo N and Chan TM (2017) Super structures: an update on high-strength-steel design. *Proceedings of the Institution of Civil Engineers - Civil Engineering* 170(4): 149.

Cao X, Zhao G, Kong Z, et al. (2020) Experimental study on local buckling of 800 MPa HSS welded I-section columns under axial compression. *Thin-Walled Structures* 155: 106878.

da Silva LS, Marques L, Tankova T, et al. (2017) *SAFE-BRICTILE: Standardization of Safety Assessment*

Procedures across Brittle to Ductile Failure Modes. Research programme of Research Fund for Coal & Steel, final report.

EN 1990:2002 (2002) Eurocode – basis of structural design.

EN 1993-1-12:2007 (2007) Eurocode 3: design of steel structures – Part 1-12: additional rules for the extension of EN 1993 up to steel grades S700.

EN 1993-1-1:2005 (2005) Eurocode 3: Design of steel structures – Part 1-1: general rules and rules for buildings.

EN 1993-1-5:2006 (2006) Eurocode 3: design of steel structures – Part 1-5: plated structural elements.

Fieber A, Gardner L and Macorini L (2019) Design of structural steel members by advanced inelastic analysis with strain limits. *Engineering Structures* 199: 109624.

Fieber A, Gardner L and Macorini L (2020) Structural steel design using second-order inelastic analysis with strain limits. *Journal of Constructional Steel Research* 168: 105980.

Gardner L (2008) The continuous strength method. *Proceedings of the Institution of Civil Engineers - Structures and Buildings* 161(3): 127–133.

Gardner L and Nethercot DA (2004) Structural stainless steel design: A new approach. *Structural Engineer* 82(21): 21–28.

Gardner L, Fieber A and Macorini L (2019) Formulae for calculating elastic local buckling stresses of full structural cross-sections. *Structures* 17: 2–20.

Gardner L, Yun X and Walport F (2023) The continuous strength method – Review and outlook. *Engineering Structures* 275: 114924.

Hibbitt HD, Karlsson BI and Sorensen EP (1997) *ABAQUS: Theory Manual*. Hibbitt, Karlsson & Sorensen.

Meng X, Gardner L, Sadowski AJ, et al. (2020) Elasto-plastic behaviour and design of semi-compact circular hollow sections. *Thin-Walled Structures* 148: 106486.

prEN 1993-1-1:2019 (2019). Eurocode 3: Design of steel structures – Part 1-1: General rules and rules for buildings.

Schafer BW and Adany S (2006) Buckling analysis of cold-formed steel members using CUFSM: conventional and constrained finite strip methods. In: Eighteenth International Specialty Conference on Cold-Formed Steel Structures, Orlando, Florida, USA, 26-27 October, 2006, pp. 39–54.

Shi G, Zhou W, Bai Y, et al. (2014) Local buckling of 460MPa high strength steel welded section stub columns under axial compression. *Journal of Constructional Steel Research* 100: 60–70.

Shi G, Zhou W and Lin C (2015) Experimental investigation on the local buckling behavior of 960 MPa high strength steel welded section stub columns. *Advances in Structural Engineering* 18(3): 423–437.

Shi G, Xu K, Ban H, et al. (2016) Local buckling behavior of welded stub columns with normal and high strength steels. *Journal of Constructional Steel Research* 119: 144–153.

Su A, Sun Y, Liang Y, et al. (2021) Experimental and numerical studies of S960 ultra-high strength steel welded I-sections under combined compression and minor-axis bending. *Engineering Structures* 243: 112675.

Su A, Sun Y, Liang Y, et al. (2021a) Membrane residual stresses and local buckling of S960 ultra-high strength steel welded I-section stub columns. *Thin-Walled Structures* 161: 107497.

Su A, Sun Y, Zhao O, et al. (2021b) Local buckling of S960 ultra-high strength steel welded I-sections subjected to combined compression and major-axis bending. *Engineering Structures* 248: 113213.

Sun Y, Liang Y and Zhao O (2019) Testing, numerical modelling and design of S690 high strength steel welded I-section stub columns. *Journal of Constructional Steel Research* 159: 521–533.

Sun Y, Liang Y, Zhao O, et al. (2021) Experimental and numerical investigations of S690 high-strength steel welded I-sections under combined compression and bending. *Journal of Structural Engineering* 147(5): 04021054.

Yun X and Gardner L (2017) Stress-strain curves for hot-rolled steels. *Journal of Constructional Steel Research* 133: 36–46.

Yun X and Gardner L (2018) The continuous strength method for the design of cold-formed steel non-slender tubular cross-sections. *Engineering Structures* 175: 549–564.

Yun X, Gardner L and Boissonnade N (2018a) The continuous strength method for the design of hot-rolled steel cross-sections. *Engineering Structures* 157: 179–191.

Yun X, Gardner L and Boissonnade N (2018b) Ultimate capacity of I-sections under combined loading – Part 2: parametric studies and CSM design. *Journal of Constructional Steel Research* 148: 265–274.

Yun X, Wang Z and Gardner L (2020) Structural performance and design of hot-rolled steel SHS and RHS under combined axial compression and bending. *Structures* 27: 1289–1298.

Yun X, Meng X and Gardner L (2022) Design of cold-formed steel SHS and RHS beam–columns considering the influence of steel grade. *Thin-Walled Structures* 171: 108600.

Yun X, Zhu YF, Meng X, et al. (2023) Welded steel I-section columns: residual stresses, testing, simulation and design. *Engineering structures* 282: 115631.

Zhu Y, Yun X and Gardner L (2023) Behaviour and design of high strength steel homogeneous and hybrid welded I-section beams. *Engineering Structures* 275: 115275.

Ziemian RD (2010) *Guide to Stability Design Criteria for Metal Structures*. Hoboken, NJ: John Wiley & Sons.